

Mineralogy and origin of oxygen-bearing platinum-iron grains based on an X-ray absorption spectroscopy study†

KÉIKO H. HATTORI,^{1,*} YOSHIO TAKAHASHI,² AND THIERRY AUGÉ³

¹Department of Earth Sciences, University of Ottawa, Ottawa, Ontario K1N 6N5, Canada

²Department of Earth and Planetary Systems Science, Hiroshima University, Higashi-Hiroshima 739-8526, Japan

³BRGM, 3 Avenue Claude-Guillemin, BP 36009, 45060 Orléans Cedex 2, France

ABSTRACT

Oxygen-bearing platinum group minerals have been reported from many locations, but their mineralogical identity has been debated. We conducted an X-ray micro-beam absorption study of O-bearing Pt-Fe grains recovered from a stream in southern New Caledonia. The Pt L_{III} -edge absorption spectrum indicates that Pt is mostly in the metallic state, not combined with O or OH⁻. The bond length between Pt and the neighboring atoms, based on the extended X-ray absorption fine structures, is much longer than the Pt-O bond length, also indicating that Pt is not bonded with O. A quantitative simulation of the atomic structure around Pt suggests that O-bearing Pt-Fe has a similar, but disturbed, structure compared to isoferroplatinum.

The absorption spectra of Fe K -edge for the studied samples have a small peak at 7122 eV and a large peak at 7128 eV. Since isoferroplatinum has a larger peak at 7122 eV, the peak at 7128 eV is explained by the presence of an Fe³⁺-bearing phase. A 10:90 mixture of ferrihydrite (Fe³⁺-O-OH) and isoferroplatinum yields the observed absorption spectra. The data suggest that the O-bearing Pt-Fe is a physical mixture of relict isoferroplatinum and newly precipitated Fe³⁺-O-OH. We suggest that O-bearing Pt-Fe formed by the dissolution of Fe⁰ followed by the dissolution of Pt⁰ from isoferroplatinum and precipitation of Fe³⁺ during weathering of host ultramafic rocks.

Keywords: XANES, EXAFS, PGM oxides, PGE, weathering, serpentinization

INTRODUCTION

Oxygen-bearing grains of platinum group minerals (PGM) have been reported in weathered rocks and placers from many locations, mostly in tropical climates. Examples include Pt-bearing oxides in Madagascar, Burma, South Africa, and Zimbabwe (Cabri et al. 1996; Hey 1999; Oberthür et al. 2003); Ir-bearing oxides from Madagascar and the Urals (Legendre and Augé 1993; Jedwab 2004); Pd oxides in Minas Gerais, Brazil, and the Aldan Shield, Russia (McDonald et al. 1999; Cabral and Lehmann 2003; Shcheka et al. 2005); and O-bearing PGM from New Caledonia (Augé and Legendre 1994). Some O-bearing PGM have been given names, such as palladinite (PdO) (McDonald et al. 1999) and irite (Ir-oxide) (Jedwab 2004), but whether they are indeed new minerals is open to debate.

Characterization of these O-bearing PGM is important to understand the mineralogy of PGM and evaluate the behavior of platinum group elements (PGE) in weathering environments. In addition, their characteristics are relevant to the design of efficient extraction techniques for PGE from lateritic rocks (Evans 2002). This paper presents an X-ray absorption study of Pt and Fe in O-bearing Pt-Fe occurrences from New Caledonia and discusses their speciation and host phases.

GEOLOGICAL SETTING AND SAMPLES

The samples were collected from a stream dissecting the Massif du Sud, a large Late Eocene ophiolite body in New Caledonia (Fig. 1a). The Massif du Sud represents the lower sequence of an ophiolite, mainly composed of residual mantle peridotites of harzburgite and dunite, with minor clinopyroxene-bearing cumulate rocks. Chromitite seams and pods are common in the ultramafic rocks, especially in the Pirogues zone, which is situated ~1 km from the ocean along the Pirogues River (Fig. 1). High contents of platinum group elements (PGE) occur in rocks associated with these chromites and in laterite cover and alluvial sediments derived from these rocks.

Platinum group minerals (PGM) in peridotites and streams reported in the area include laurite (RuS₂), Ir-Cu sulfides, isoferroplatinum (Pt₃Fe), tulameenite (Pt₂FeCu), native Pt, alloys of Os-Ir-Ru, cooperite (PtS), and sperrylite (PtAs₂). Among these minerals isoferroplatinum (Pt₃Fe) is the most abundant mineral both in rocks and alluvial grains in placers (Augé and Legendre 1994; Augé and Maurizot 1995).

Sample grains used for this study were alluvial grains collected from a small stream in the Pirogues zone, draining lateritic soils and unweathered ultramafic rocks (Fig. 1). O-bearing PGM grains are abundant in magnetic fractions of heavy minerals from which the studied grains were obtained. The grains were mounted in epoxy resin (2 mm in thickness) for optical examination under an incident light microscope, and electron microprobe analysis, as well as for this X-ray absorption study. These O-bearing

* E-mail: khattori@uottawa.ca

† Open access, thanks to authors' generous funding. Article available to all readers on GSW (<http://ammin.geoscienceworld.org>).

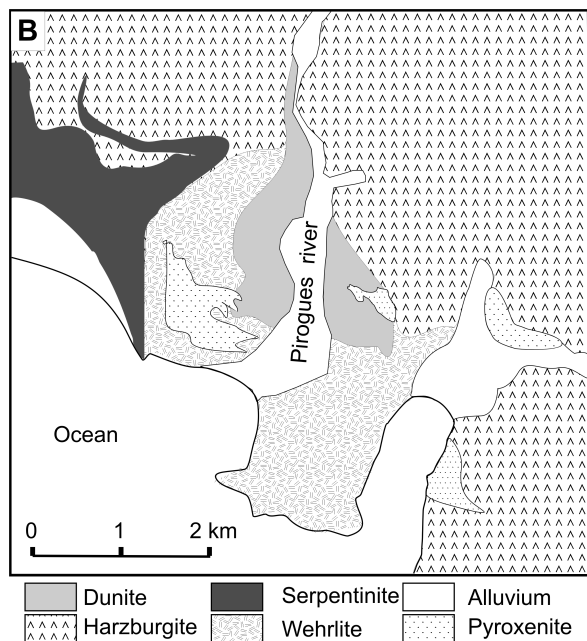
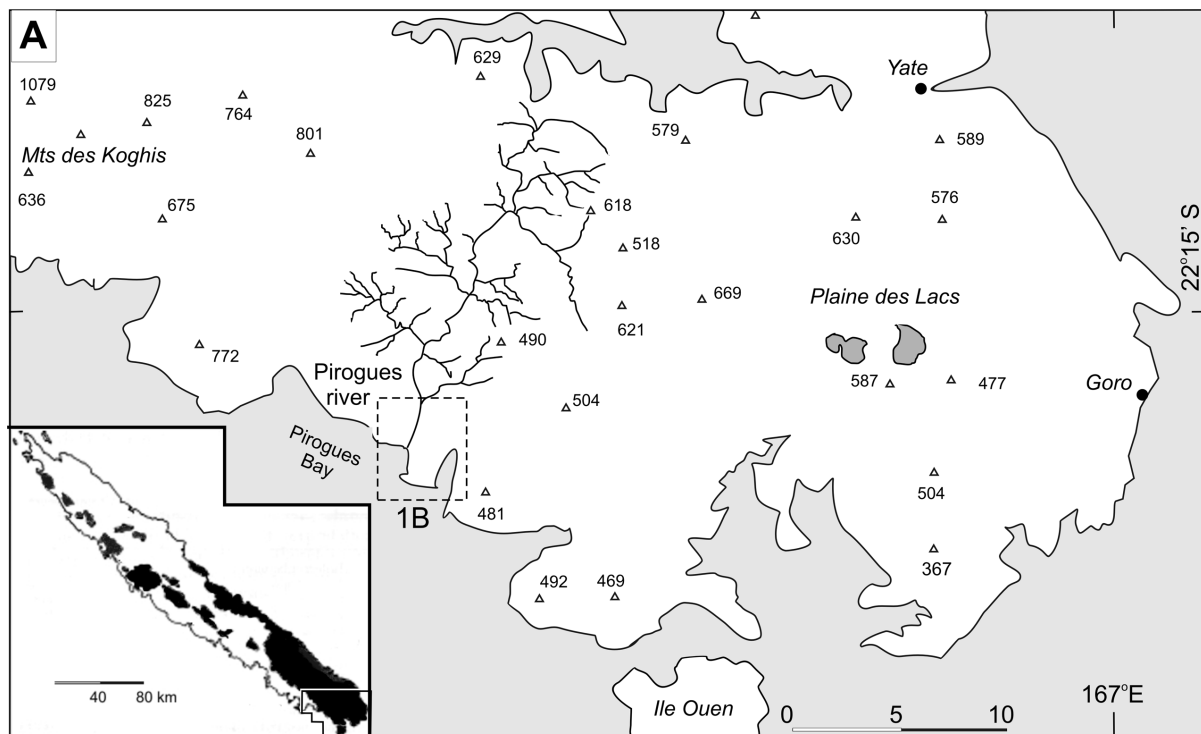


FIGURE 1. Topography and simplified geology of the study area in southwestern New Caledonia. The distribution of ultramafic rocks in New Caledonia is shown in solid black in the insert. The geologic map is modified after Augé and Maurizot (1995).

X-ray micro-beam absorption study. Grain 3 has been described as Grain 3B3 by Augé and Legendre (1994) and Grain 4 is a typical porous grain of O-bearing Pt-Fe from the area.

EXPERIMENTAL METHODS

Chemical compositions of PGM, including O, were determined with a Cameca SX electron microprobe. The analytical conditions were: accelerating voltage 25 kV, beam current 20 nA, and counting time 6 s. The standards were Cr_2O_3 (Cr), GaAs (As), and pure metals for all other elements. Oxygen contents were determined by the counts of $\text{OK}\alpha$ peak with an accelerating voltage of 10 kV. To make sure that oxygen is from PGM, rather than from epoxy, Cl contents were monitored during the analyses. Backscattered electron images and secondary electron images were taken with a JEOL 6400 digital scanning electron microscope equipped with a Link X-ray analyzer.

X-ray absorption spectra were obtained from sample grains mounted in epoxy resin. X-ray absorption spectra of the Pt L_{III} -edge were measured at BL37XU X-ray beam line of SPring-8 in Hyogo, Japan, and those of the Fe K -edge at BL-4A X-ray beam line of Photon Factory in Tsukuba, Japan. The incident X-ray beam was monochromatized using a Si (111) double-crystal monochromator. The beam size on the sample surface was $100 \times 100 \mu\text{m}$ for Pt L_{III} -edge and $7 \times 5 \mu\text{m}$ for Fe K -edge measurement. We selected the small beam size for Fe to make sure that the absorption spectra are obtained from specific areas of grains, without interference from other grains. The small grain size, however, resulted in low counts and absorption spectra of less than ideal quality.

Absorption spectra were recorded under ambient conditions ($\sim 20^\circ\text{C}$, 1 bar), and recorded using a 19-element Ge semiconductor detector by scanning the incident X-ray energy at ~ 0.35 eV steps. The Pt L_{III} -edge spectra were collected in the fluorescence mode and Fe K -edge spectra in transmission mode. Reference materials for Pt L_{III} -edge absorbance included Pt^{4+}O_2 , Pt^{2+} -acetylacetonato complex, Pt metal, and isoferroplatinum. The first two were purchased from Wako Pure Chemicals Inc., Osaka, Japan, and Pt-metal foil was from Nilano Corporation Inc.,

grains show much lower reflectivity than isoferroplatinum and noticeable pleochroism and anisotropy under regular incident light microscope (Figs. 2a and 2c). Some O-bearing grains show concentric zoning under the microscope (Fig. 2a) and in backscattered electron images (Fig. 2b), with darker zones corresponding to low-Pt and high-Fe contents. Some have cracks and are porous, especially on the margins of grains (Figs. 2c and 2d). We selected two representative grains, Grains 3 and 4, for our

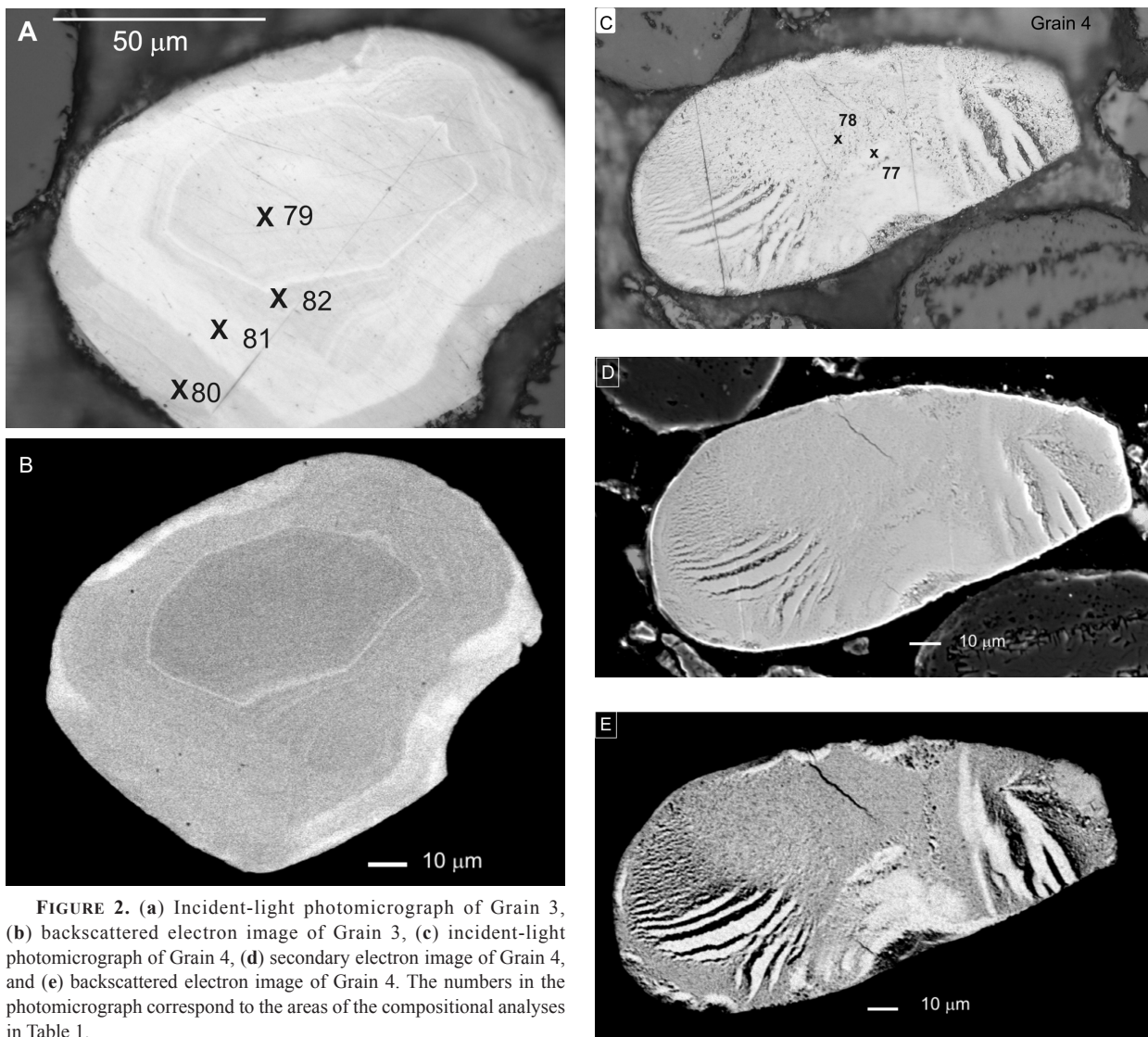


FIGURE 2. (a) Incident-light photomicrograph of Grain 3, (b) backscattered electron image of Grain 3, (c) incident-light photomicrograph of Grain 4, (d) secondary electron image of Grain 4, and (e) backscattered electron image of Grain 4. The numbers in the photomicrograph correspond to the areas of the compositional analyses in Table 1.

Tokyo, Japan. The isoferroplatinum grain is of alluvial origin from the Omutnaya River, Urals, and was described by Hattori and Cabri (1992). Reference materials for Fe included hematite (Fe_2O_3), magnetite ($\text{Fe}^{2+}\text{Fe}^{3+}\text{O}_4$), goethite [$\alpha\text{-Fe}^{3+}\text{O}(\text{OH})$], ferrihydrite ($\text{Fe}^{3+}\text{-O-OH}$), Fe metal, and the isoferroplatinum grain. Fe metal foil was purchased from Nilano Corporation Inc. Other Fe reference materials were synthesized following the method described by Cornell and Schwertmann (2003). Most samples were scanned twice and samples with significant noise in the spectra were subjected to a third scanning. The peak position of reference materials did not drift more than 0.35 eV throughout this study. The background absorption, estimated from a pre-edge region, was subtracted using a linear function. Energy was calibrated by defining the main absorbance peak of Pt metal at 11 564 eV for Pt L_{III} -edge absorption experiments. For the Fe K -edge spectrum collection, the pre-edge peak of hematite was defined as 7110.5 eV.

Extended X-ray absorption fine structure (EXAFS) was recorded from 11 250 to 11 950 eV to cover the k value ranging from 0 to 11 \AA^{-1} at the Pt L_{III} -edge, and from 7000 to 7700 eV for the k value from 0 to 12 \AA^{-1} at the Fe K -edge. The data were analyzed using the Rigaku REX 2000 program (version 2.3) and FEFF 7.0 (Zabinsky et al. 1995; Ankudinov and Rehr 1997), after the initial structural data were obtained with the ATOMS program (Ravel 2001) using crystallographic data for isoferroplatinum from Cabri and Feather (1975). Smooth absorption of the Pt free atom (μ_0) in the EXAFS region was removed using five cubic spline curves following subtraction of background and normalization to the edge values. The

energy unit was transformed from eV to \AA^{-1} to produce the EXAFS function $\chi(k)$, where k (\AA^{-1}) is the photoelectron wave vector given by

$$\sqrt{2m(E - E_0 / h^2)};$$

E is the energy of the incident X-ray and E_0 the threshold energy. The E_0 value was determined from the maximum value in the first derivative in the absorption edge region. The k^3 -weighted EXAFS function, $k^3\chi(k)$, was Fourier transformed from k space ($1/\text{\AA}$) into R space (\AA) over the value of k ranging from 3.75 to 10.4 \AA^{-1} , which yielded a radial structure function.

RESULTS

Chemical composition

The studied grains show significant compositional variations within individual grains and among different grains (Figs. 2 and 3). The compositional heterogeneity is apparent under incident light microscopy and in backscattered electron images (Fig. 2). Platinum is the most abundant element, ranging from 72 to 89.7 wt%, which is lower than the Pt content, 91.3 wt%, of the

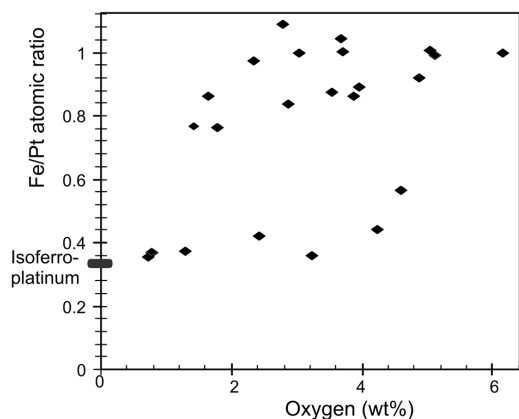


FIGURE 3. Fe/Pt atomic ratios vs. O contents of grains in the same magnetic, heavy fraction. The ratio of Fe/Pt of the ideal formula of isoferroplatinum is shown. The ratios are commonly low for natural isoferroplatinum due to incorporation of Ni and Cu in the Fe site.

TABLE 1. Chemical compositions of O-bearing Pt-Fe grains used for X-ray absorption study

	Ideal	Referent†	Studied grains					
	formula	isoferroplatinum	Gr. 3	Gr. 3	Gr. 3	Gr. 3	Gr. 4	Gr. 4
Anal. no.*			79*	82*	81*	80	78*	77*
		center				rim*		
Ir (wt%)		2.39	0.32	<0.02	0.25	0.04	0.12	0.11
Ru			<0.01	<0.02	0.07	0.14	<0.02	<0.02
Fe	8.72	7.97	21.5	18.8	22.8	19.7	18.6	18.0
As			<0.02	<0.02	<0.02	<0.02	<0.02	0.18
Pt	91.3	88.99	72.0	73.6	73.0	74.7	75.2	73.2
Rh		0.16	0.41	0.32	0.16	0.14	0.37	0.06
Cu		0.49	0.11	0.08	0.14	0.10	0.98	0.91
Ni			0.49	0.26	0.39	0.25	0.30	0.38
Pd			0.78	1.17	0.61	0.62	1.55	2.11
Mn			<0.02	<0.02	<0.02	0.05	0.49	0.32
Os			<0.02	<0.02	<0.02	<0.02	<0.02	<0.02
Cr			<0.02	0.02	<0.02	0.31	0.03	0.02
O			3.67	3.96	2.79	4.88	1.65	3.88
Sum		100.0	99.26	98.23	100.20	100.93	99.27	99.15
Ir (at%)	0.00	2.0	0.166	0.00	0.134	0.020	0.065	0.058
Ru	0.00		0.00	0.00	0.071	0.130	0.00	0.00
Fe total	25.0	23.0	38.2	34.3	41.8	33.2	34.4	32.6
As	0.00		0.00	0.00	0.00	0.00	0.00	0.242
Pt	75.0	73.5	36.7	38.5	38.4	36.1	39.9	37.9
Rh	0.00	0.25	0.396	0.316	0.159	0.128	10.4	0.059
Cu	0.00	1.2	0.172	0.128	0.226	0.148	1.60	1.45
Ni	0.00		0.830	0.451	0.682	0.401	0.529	0.653
Pd	0.00		0.729	1.120	0.588	0.549	1.51	2.00
Mn	0.00		0.00	0.00	0.00	0.086	0.922	0.588
Cr	0.00		0.00	0.039	0.00	0.561	0.060	0.039
atom Fe/Pt	0.333	0.313	1.04	0.893	1.09	0.917	0.862	0.862
% of Fe ³⁺ ‡			19.9	24.5	14.3	28.8	10.3	25.0
% of metallic Fe	100		80.1	75.5	85.7	71.2	89.7	75.0

* Analysis locations are shown in Figure 2.

† No. 53 grain in Hattori and Cabri (1991).

‡ The amount of Fe³⁺ is calculated from the amount of O and the formula ferrihydrite, Fe₃²⁺(O,OH,H₂O)₁₂, by Eggleton and Fitzpatrick (1988).

ideal formula for isoferroplatinum (Table 1). The atomic ratios of Fe/Pt are higher than the value, 0.33, of the ideal formula of isoferroplatinum, and vary within a grain ranging from 0.35 to 1.1. There is no apparent correlation between these ratios and the oxygen contents (Fig. 3). Contents of O vary up to 6.2 wt% in the magnetic heavy fractions (Fig. 3).

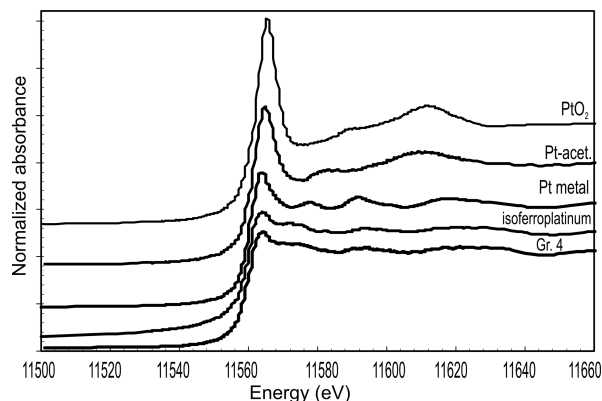


FIGURE 4. Platinum L_{III} -edge XANES spectra of Pt-Fe-oxide grain (Grain 4), and reference materials including Pt⁴⁺O₂, Pt²⁺-acetylacetonato complex (Pt-Acet), Pt metal, and isoferroplatinum (Pt₃Fe). The X-ray absorption (μ) is defined as the ratio of fluorescence X-ray intensity (I_f) to the incident X-ray intensity (I_0).

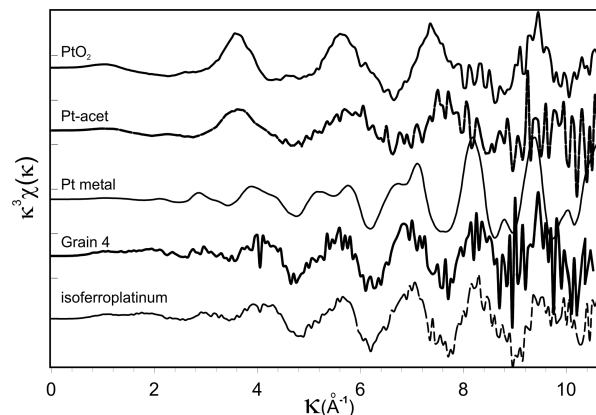


FIGURE 5. The $k^3\chi(k)$ function of Pt derived from EXAFS spectroscopy data. The spectrum of Grain 4 is compared to the spectra of isoferroplatinum, Pt metal, Pt²⁺-acetylacetonato complex (Pt-acet), and Pt⁴⁺O₂. Note that the pattern of the sample is similar to that of isoferroplatinum.

Valence and atomic environment of platinum

The X-ray absorption near-edge structure (XANES) of Pt in the studied grains shows a sharp absorption peak of Pt L_{III} at around 11565 eV (Fig. 4), and the observed spectra are similar to that of isoferroplatinum (Pt₃Fe), in which Pt is in a metallic state (Fig. 4). The absorption edge of studied grains is also similar to that of Pt metal (Fig. 4) and is located in a lower energy site than those for Pt²⁺-acetylacetonato complex and Pt⁴⁺O₂, in which Pt is combined with O in divalent and tetravalent conditions, respectively. The data indicate that the majority of Pt in O-bearing Pt-Fe is in a metallic state.

The neighboring atoms of Pt in Grain 4 were evaluated using the EXAFS data. The $k^3\chi(k)$ function of Grain 4 is compared to those of reference materials (Fig. 5). The value of studied grains is very similar to that of isoferroplatinum, indicating that the local atomic environment of Pt in the grains is similar to that in isoferroplatinum, where Pt⁰ is surrounded by Pt⁰ and Fe⁰. The

$k^3\chi(k)$ function of the phase is distinctly different from those of Pt^{2+} -acetylacetonato complex and Pt^{4+}O_2 (Fig. 5).

Radial structure functions of Pt based on the EXAFS data yield the values, $R+\Delta R$ (Fig. 6), which approximate the distances between Pt and the neighboring atoms. The values of the Pt^{2+} -acetylacetonato complex and Pt^{4+}O_2 are short, $<2 \text{ \AA}$, where Pt is bonded with O (Fig. 6). The value of the studied grains is much larger than 2 \AA , indicating that O atoms are not the principal neighbors of Pt in the sample. Instead, the value is similar to that for isoferroplatinum, where Fe^0 and Pt^0 are the atoms that neighbor Pt^0 .

To confirm the proposed interpretation, we carried out a quantitative evaluation of the local atomic structure of Pt, using the EXAFS-fitted parameters derived from FEFF. The simulation successfully produced the values of $k^3\chi(k)$ and radial structural function for Grain 4 (Fig. 7), and reference isoferroplatinum. The values of the reference are similar to those of isoferroplatinum based on the crystallographic study by Cabri and Feather (1975) (Table 2), verifying the simulation. Grain 4 yielded a bond length of 2.639 \AA for Pt-Fe and 2.756 \AA for Pt-Pt (Table 2). The bond length of Pt-Pt is very similar to the value, 2.752 \AA , of reference isoferroplatinum, but the length of Pt-Fe is slightly shorter than

the value, 2.714 \AA , of reference isoferroplatinum. The values of the studied grain are much longer than the Pt-O bond length, which is 1.6 \AA for Pt^{4+}O_2 . The data confirm a metallic state of Pt in Grain 4. Similar bond lengths between the studied material and isoferroplatinum suggest that the two have similar local atomic structures.

The simulation yielded coordination numbers of 3.5 for Pt-Fe and 3.1 for Pt-Pt (Table 2). The coordination numbers are significantly lower than the values of 4 and 8, respectively, for isoferroplatinum (Table 2), suggesting that the crystal structure of the studied grain is significantly disordered relative to isoferroplatinum.

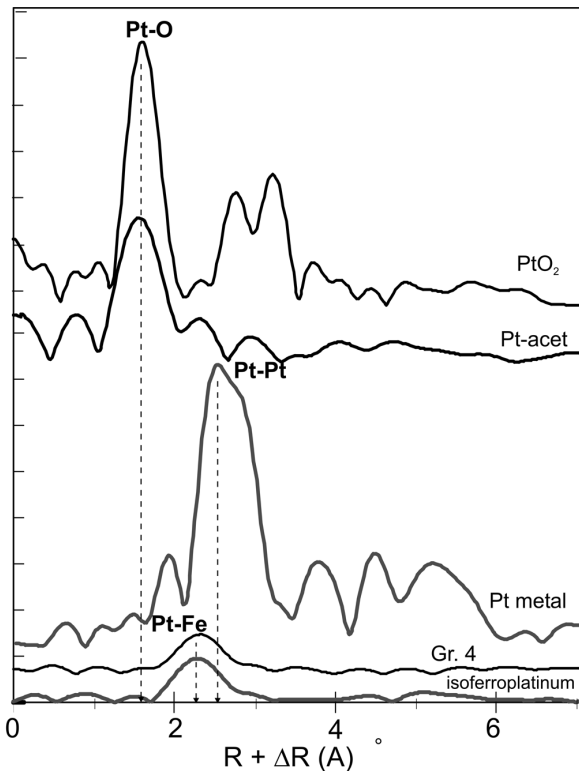


FIGURE 6. Radial structural function spectra of Pt, obtained from EXAFS spectroscopy data. Spectrum of Grain 4 is compared to those of isoferroplatinum (Pt-Fe), Pt^{2+} -acetylacetonato complex (Pt-acet), and Pt^{4+}O_2 . Note the small values of $R+\Delta R$, $<2 \text{ \AA}$, for Pt^{4+}O_2 and Pt^{2+} -acetylacetonato complex, where Pt is bonded with O. The values of $R+\Delta R$ approximate the bond length between Pt and the neighboring atoms, but are longer than the true lengths because Fourier transformation is not corrected for the phase shift.

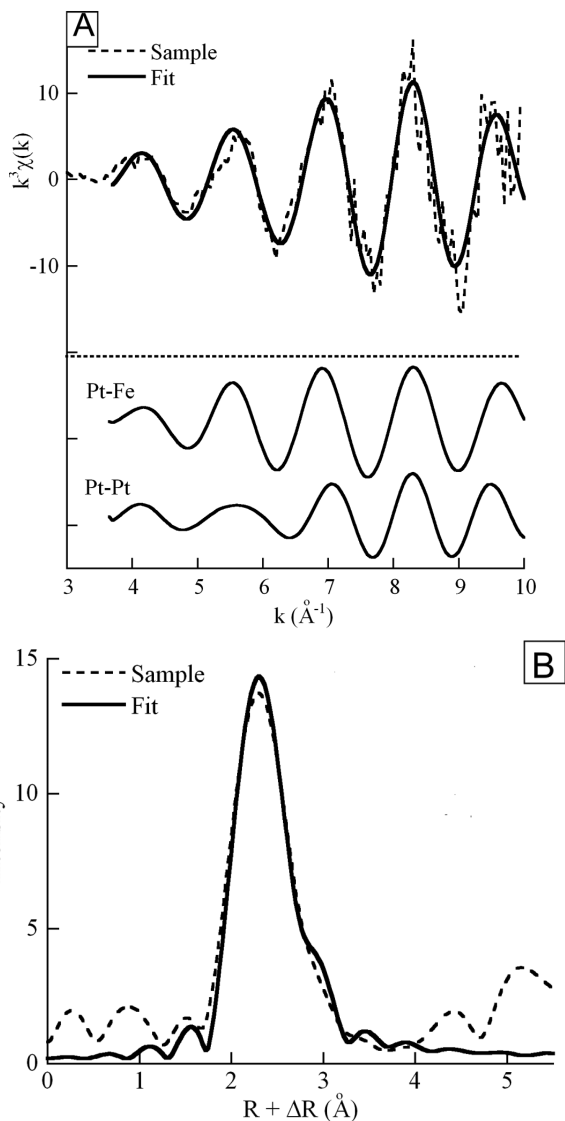


FIGURE 7. (a) Simulation of EXAFS spectra of Pt in Grain 4 using parameters obtained from FEFF 7.02. Dashed lines show the original EXAFS data, and solid lines are the fitted spectrum. The contributions of Pt-Fe and Pt-Pt to the fitted spectrum are shown in the lower box. (b) Fourier-transformed data of Pt-EXAFS spectra showing the radial distribution of atoms at a distance of 2.7 \AA around Pt.

TABLE 2. Local atomic structures of Pt and Fe calculated based on extended X-ray absorption fine structure (EXAFS) spectra

Sample	Edge	Calculation based on EXAFS spectra						Crystallographic data*		
		Analyzed	Shell	CN	<i>R</i> (Å)	ΔE_0 (eV)	σ^2 ($\times 10^3$)	Shell	CN	<i>R</i> (Å)
isoferroplatinum	Pt L_{III}	2 shells	Pt-Fe	3.2	2.714	8.7	1.3	Pt-Fe	4	2.732
			Pt-Pt	7.3	2.752			Pt-Pt	8	
Grain 4	Pt L_{III}	2 shells	Pt-Fe	3.5	2.639	4.3	1.5			
			Pt-Pt	3.1	2.756					
Grain 3	Fe <i>K</i>	2 shells	Fe-Pt	6.4	2.614	-1.5	8.6	Fe-Pt	12	2.732
			Fe-Fe	1.4	2.666					
Grain 4	Fe <i>K</i>	2 shells	Fe-Pt	5.7	2.640	-2.9	6.7			
			Fe-Fe	2.1	2.681					
metallic Fe	Fe <i>K</i>	2 shells	Fe-Fe	9.0	2.489	9.5	7.4	Fe-Fe	8	2.499
			Fe-Fe	5.0	2.855			15.1	Fe-Fe	6

Notes: CN = coordination number, *R* = interatomic distance, ΔE_0 = threshold E_0 shift, σ = Debye-Waller mean-square disorder parameter. Errors in the fitted parameters were ≤ 0.02 Å for *R*, and $\leq 20\%$ for σ^2 (O'Day et al. 1994).

* Sources of crystallographic data: isoferroplatinum (Cabri and Feather 1975) and metallic Fe (Basinski et al. 1955).

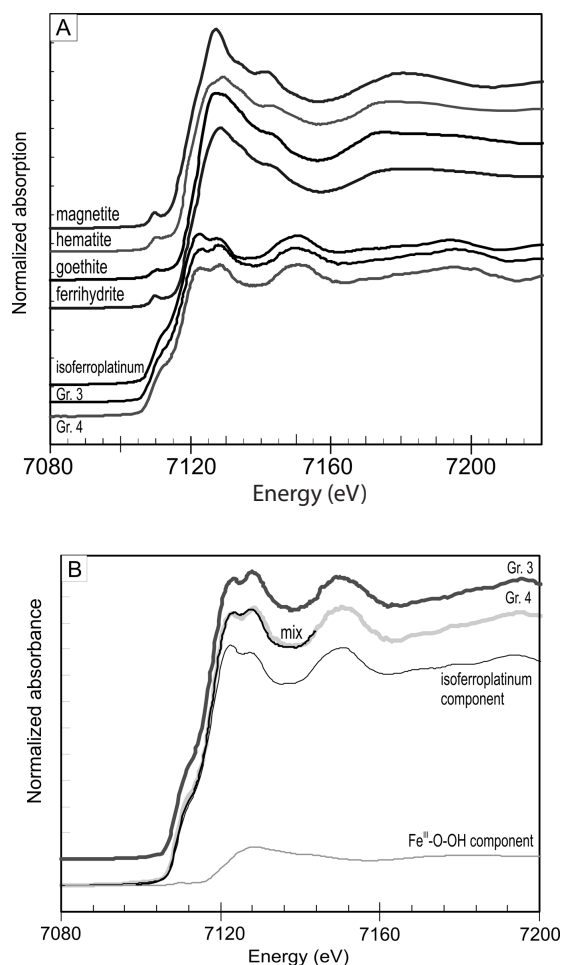


FIGURE 8. (a) Normalized Fe *K*-edge XANES spectra of sample grains, isoferroplatinum, magnetite, hematite, goethite, and ferrihydrite. Note that Pt-Fe “oxide” grains have similar spectra as isoferroplatinum, but that isoferroplatinum has higher peak at 7122 eV than at 7128 eV. (b) The curve “mix” is a hypothetical spectrum of a 10:90 mixture of isoferroplatinum and ferrihydrite and the contribution of the two components to the mixture are shown as thin lines. The spectrum of the mixture fits well with the observed spectrum of Grain 4. For the clarity of the diagram, another mixture is not shown, but the spectrum of Grain 3 fits well with an 11:89 mixture of isoferroplatinum and ferrihydrite.

X-ray absorption data of iron

The X-ray absorption spectra of the Fe *K*-edge of the two sample grains are almost identical and very similar to that of isoferroplatinum. All show absorption peaks at 7122 and 7128 eV (Fig. 8a). Similar spectra suggest that the overall local atomic structure around Fe is similar among the samples and isoferroplatinum.

A close examination of the absorption spectra, however, reveals distinct differences between the studied grains and isoferroplatinum. The samples show a greater absorption at 7128 eV than at 7122 eV, whereas isoferroplatinum shows a greater absorption at 7122 eV (Fig. 8b). The data suggest the presence of another phase contributing to the absorption peak at 7128 eV.

A quantitative simulation of the local atomic structure of Fe yielded Fe-Pt bond lengths of 2.614 Å for Grain 4 and 2.640 Å for Grain 3 (Table 2). The values are smaller than that of isoferroplatinum, 2.732 Å based on the crystallographic study by Cabri and Feather (1975), but Cabri and Feather (1975) noted that the unit cell of isoferroplatinum varies and decreases with increasing Fe. Similar to Pt, the coordination numbers of Fe are significantly lower than those of isoferroplatinum (Table 2), which suggests that the atomic structure around Fe is also disordered. Furthermore, Fe in the studied grains is surrounded by significant amount of Fe (Table 2). It is possible that isoferroplatinum may be partially changed to a high-Fe form of Fe-Pt alloy, tetraferroplatinum (FePt), which is a common alteration phase of isoferroplatinum. Alternatively, this may simply reflect the disordered nature of the studied isoferroplatinum. Alloys commonly form disordered crystals where metals do not reside at specific sites (e.g., Cabri and Feather 1975).

DISCUSSION

Oxygen-bearing phase

The Fe *K*-edge X-ray absorption spectra show that O-bearing Pt-Fe contains at least two phases: isoferroplatinum and a second phase. Considering that the electron microprobe data show the grains are composed of Fe, Pt, and O (Table 1), there are very few possibilities for this second phase. They include Fe oxide, Fe hydroxides, and Fe carbonates, since carbon and hydrogen are not detected by the electron microprobe. The possible minerals are magnetite ($\text{Fe}^{2+}\text{Fe}_3^+\text{O}_4$), siderite ($\text{Fe}^{2+}\text{CO}_3$), maghemite (Fe_3^+O_3), hematite (Fe^{3+}O_3), goethite [$\alpha\text{-Fe}^{3+}\text{O}(\text{OH})$], lepidocrocite ($\gamma\text{-Fe}^{3+}\text{OOH}$), and ferrihydrite ($\text{Fe}^{3+}\text{-O-OH}$). Among

them, we discount Fe^{2+} -bearing phases because they do not show a large absorption peak at 7128 eV (Fig. 8a). The spectra of magnetite, maghemite, and hematite suggest that they are also unlikely candidates. The remaining possible phases are goethite [$\alpha\text{-Fe}^{3+}\text{O}(\text{OH})$], lepidocrocite [$\gamma\text{-Fe}^{3+}\text{O}(\text{OH})$], and ferrihydrite ($\text{Fe}^{3+}\text{-O-OH}$). Therefore, we calculated absorption spectra of hypothetical mixtures of isoferroplatinum and each of these phases. The results show that mixtures containing ferrihydrite give the best-fit patterns to those observed (Fig. 8b). The absorption spectrum of Grain 3 fits well with that of a 10:90 mixture of ferrihydrite and isoferroplatinum (Fig. 8b), and the spectrum of Grain 4 by an 11:89 mixture. Although our data cannot discount the presence of other Fe^{3+} -bearing phases, the proposed interpretation is reasonable considering that ferrihydrite is the most common Fe phase in surface environments (Cornell and Schwertmann 2003).

Mineralogy of O-bearing Pt-Fe

The use of a micro-beam allowed us to obtain spectra from target areas in grains, but this resulted in lower counts and quality of data than the results using large beams. Yet, XANES data of Pt are sufficiently clear to indicate that the majority of Pt atoms in studied grains are in a metallic state. The absorption data of Fe show significant Fe as Fe^{3+} in $\text{Fe}^{3+}\text{-O-OH}$, which is most likely ferrihydrite.

The presence of ferrihydrite is consistent with the occurrence of the samples from a stream and in weathered ultramafic rocks in southern New Caledonia, because ferrihydrite is the most common Fe phase formed in soil and stream sediments (Cornell and Schwertmann 2003). The presence of ferrihydrite is further supported by its magnetic property, as the sample grains are recovered from magnetic fractions of heavy mineral concentrates. Isoferroplatinum is isometric and not magnetic (Cabri 2002), but ferrihydrite is magnetic (e.g., Karapinar 2003).

The occurrence of ferrihydrite is also consistent with the low reflectivity of the studied grains (Fig. 2). Metal alloys in general have high reflectivity and oxides have low reflectivity. Hydrated oxide phases have even lower reflectance than anhydrous oxides (Ramdohr 1980). The reflectivity of isoferroplatinum is >60% (Cabri 2002), and that of goethite is <17% (Ramdohr 1980).

The abundance of Fe^{3+} in the samples is evaluated from their O contents and the ratios of O/Fe in ferrihydrite, $\text{Fe}_3^+(\text{O}, \text{OH}, \text{H}_2\text{O})_{12}$ (Eggleton and Fitzpatrick 1988). The calculation yielded fractions of Fe^{3+} ranging between 0.14 and 0.30 in Grain 3 and 0.1 and 0.25 in Grain 4 (Table 2). Although the values are approximate because of uncertainty of the formula of ferrihydrite (Cornell and Schwertmann 2003), the calculation suggests that the amount of metallic Fe^0 is far greater than Fe^{3+} in the sample grains. This is consistent with the Fe *K*-edge spectra of sample grains that are similar to that of isoferroplatinum (Fig. 8b).

Precursor mineral of oxygen-bearing Pt-Fe

A possible precursor mineral for O-bearing Pt-Fe can be evaluated from the reported occurrences of PGM in unweathered rocks in the Pirogues River area. They are laurite (RuS_2), Ir-Cu sulfides, tulameenite (Pt_2FeCu), alloys of Os-Ir-Ru, cooperite (PtS), braggite [(Pt, Pd, Ni)S], isoferroplatinum, and sperrylite (PtAs_2) (Augé and Legendre 1994). Among them, sperrylite

has a pyrite-like crystal structure in which two As atoms form a dianion and combine with Pt^{2+} . Platinum in braggite occurs as a divalent cation, Pt^{2+} , and bonds ionically with S^{2-} . If these arsenide and sulfide minerals were to be transformed to other phases, Pt should be at least partially divalent and retain the atomic structure of these original minerals. Our X-ray absorption data show that Pt is in a metallic state (Fig. 4). This leaves tulameenite, tetraferroplatinum, and isoferroplatinum as possible precursors of O-bearing Pt-Fe.

Both Pt *L*_{III}-edge and Fe *K*-edge spectra of the sample grains are similar to those of isoferroplatinum, suggesting that the local atomic structures around Pt and Fe are similar to those of isoferroplatinum. It would be fortuitous for Pt to acquire a similar local atomic structure to that of isoferroplatinum unless the latter were the precursor phase. Therefore, this further supports the evidence that O-bearing phases originated from isoferroplatinum.

Although X-ray absorption spectra cannot discount the possible presence of tetraferroplatinum and tulameenite, it is unlikely that they were the precursors of the studied material because these two minerals are rare. In addition, tetraferroplatinum is considered a low-temperature alteration product of isoferroplatinum (Cabri 2002; Weiser 2002).

The contents of Cu and Ni in the O-bearing Pt-Fe are also consistent with the proposed interpretation. Isoferroplatinum may contain significant amounts of Cu (up to 6.1 wt%) and Ni (up to 5.9 wt%) (Cabri 2002), but isoferroplatinum in unweathered rocks in the studied area contains low Cu (up to 1 wt%) and Ni (up to 0.5 wt%; Augé and Maurizot 1995). Thus, the low contents of these elements in O-bearing Pt-Fe likely reflect those of the original phase.

Transformation of isoferroplatinum to form O-bearing Pt-Fe

The occurrences of O-bearing PGM are restricted to highly weathered ultramafic rocks and alluvial placers in New Caledonia and elsewhere in the world. Therefore, it is reasonable to assume that these O-bearing PGM formed during the weathering of rocks and/or the sedimentation of grains in alluvial environments. Southern New Caledonia is located at the boundary between the tropical and semi-tropical zones, and trade winds from the southeast bring much precipitation, >1100 mm/year (Vincent et al. 2007). Abundant precipitation and warm temperatures are conducive to intense chemical weathering of rocks, and the high relief of the area contributes to active, mechanical erosion.

The rocks in the area are mostly dunite and harzburgite (Fig. 1) in which olivine and orthopyroxene are the predominant minerals. These minerals are highly susceptible to weathering even at low temperatures, and the weathering produces alkaline waters and reduced gases, such as H_2 and CH_4 (Sleep et al. 2004; Abrajano et al. 1988; Sader et al. 2007; Hattori and Hamilton 2008). Surface and ground waters with a pH > 11 are common in ultramafic terrane (e.g., Barnes et al. 1967; Abrajano et al. 1990). The pH values and oxidation states vary primarily depending on rock/water ratios. The greater the ratio of rock/water, the more alkaline the water, as its composition is controlled by rocks (e.g., Palandri and Reed 2004). The evidence suggests that the rocks weather under alkaline and reduced oxidation condition at deep levels.

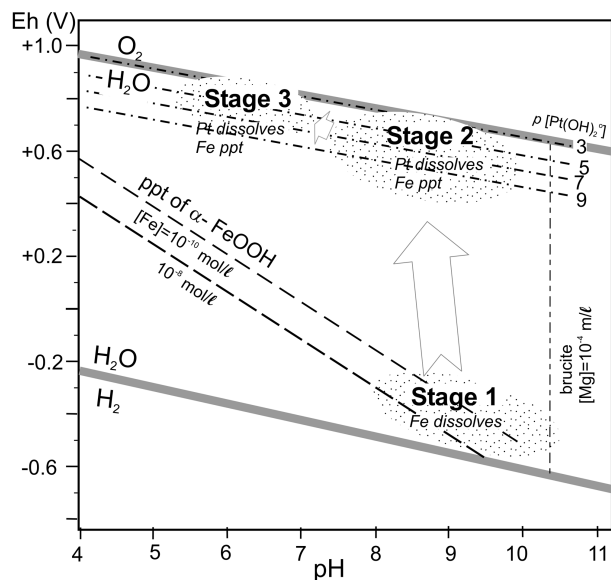
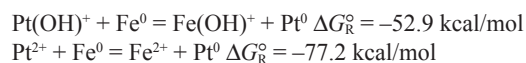


FIGURE 9. Schematic path on an Eh-pH diagram of the weathering environment of isoferroplatinum in ultramafic rocks. The precipitation of $\text{Fe}^{3+}\text{-O-OH}$ is shown for the activities of Fe^{2+} at 10^{-8} and 10^{-10} mol/L. The dash-dot lines represent activity contours of $-\log[\text{activity of Pt(OH)}_2^0]$ at 10^{-3} and 10^{-5} mol/L. Although there are large uncertainties in the thermodynamic data and the formation constants of Pt-OH complexes (discussion in Byrne 2003), the contours show increasing solubility of Pt in more oxidized water. Soluble Pt(OH)^+ is not considered since Pt(OH)_2^0 is generally considered to be the predominant Pt-OH species over a wide pH range in dilute waters (e.g., Sassani and Shock 1998; Wood 1991; Wood et al. 1992). The calculation used 61.6 kcal/mol for the standard Gibbs free energies (ΔG_f°) of Pt^{2+} (Sassani and Shock 1998) and 28.8 kcal/mol for the cumulative stability constant of Pt(OH)_2^0 (Azaroual et al. 2001). The latter values are similar to those reported by Wood (1991) and Wood et al. (1989).

Behavior of Pt and Fe during weathering. Metallic Fe^0 is not stable with liquid water and readily oxidizes to Fe^{2+} . It further oxidizes to Fe^{3+} in oxygenated water and precipitates as ferrihydrite (Fig. 9). Metallic Pt^0 is very stable under surface conditions because dissolution requires the oxidation of metallic Pt^0 , which requires a highly oxidizing environment. Once Pt^0 is oxidized to Pt^{2+} , it forms soluble OH-complexes, $\text{Pt}^{2+}(\text{OH})^+$ and neutral $\text{Pt}^{2+}(\text{OH})_2$ (Westland 1981; Wood 1991; Sassani and Shock 1998; Azaroual et al. 2001). Although there are large uncertainties in thermodynamic data and formation constants of soluble $\text{Pt}^{2+}\text{-OH}$ complexes, especially that for $\text{Pt}^{2+}(\text{OH})^+$ (Byrne 2003), it has been agreed that Pt has a high solubility as $\text{Pt}^{2+}\text{-OH}$ complexes in oxygenated water (e.g., Wood 1991; Wood et al. 1992; Azaroual et al. 2001).

Dissolved Pt may change back to the metallic state if metallic Fe is present.



The large negative value of the Gibbs standard free energy for these reactions suggests that Pt^0 is not easily oxidized in the presence of metallic Fe^0 . This suggests that the dissolution and

removal of Pt^0 and Fe^0 from isoferroplatinum may have taken place during different stages.

Formation of oxygen-bearing Pt-Fe grains during weathering. The mobility of Pt and Fe and the redox condition of water suggest the following sequence of events for the formation of O-bearing Pt-Fe grains. In Stage 1 within ultramafic rocks, alkaline waters that are highly reduced oxidation condition can remove Fe^0 from isoferroplatinum as Fe^{2+} (Fig. 9). The removal of Fe^0 likely produces the porous texture and shrinkage cracks of isoferroplatinum grains, common in the study area. During this stage, Pt^0 is stable and likely remains in isoferroplatinum. Further erosion of rocks leads to an incursion of oxygenated surface water (Stage 2 in Fig. 9). The oxygenated, alkaline water dissolves Pt^0 and washes Pt away as soluble $\text{Pt}^{2+}\text{-OH}$ complexes. Fe^{2+} in solution starts to precipitate in voids as $\text{Fe}^{3+}\text{-O-OH}$. This simultaneous dissolution of Pt^0 and precipitation of $\text{Fe}^{3+}\text{-O-OH}$ likely produced a delicate mixture of isoferroplatinum and $\text{Fe}^{3+}\text{-O-OH}$. Further weathering results in the mechanical erosion of grains from rocks, to then be exposed to fully oxygenated water at a near neutral pH in the drainage (Stage 3 in Fig. 9). The oxygenated stream water may remove more Pt^0 and continue precipitating $\text{Fe}^{3+}\text{-O-OH}$. Finally, $\text{Fe}^{3+}\text{-O-OH}$ coats the entire grains, as commonly observed in many alluvial PGM grains in the area.

ACKNOWLEDGMENTS

We thank Monika Wilk-Alemany for sample preparation and Peter Jones for his help during the SEM work. The work was supported by grants from Natural Science and Engineering Research Council of Canada to K.H.H., the Ministry of Education, Science, Sports and Culture of Japan to Y.T., and the Bureau de Recherches Géologiques et Minières of France to T.A. This work was carried out with the approval of SPring 8/JASRI (Proposal number: 2004B0169 and 2005B0181). We thank Laurence Garvie (Associate Editor), Louis J. Cabri, and one anonymous journal referee for their reviews.

REFERENCES CITED

- Abrajano, T.A., Sturchio, N.C., Bohlke, J.K., Lyon, G.L., Poreda, J., and Stevens, C.M. (1988) Methane hydrogen gas seeps, Zambales ophiolite, Philippines, deep or shallow origin? *Chemical Geology*, 71, 211–222.
- Abrajano, T.A., Sturchio, N.C., Kennedy, B.M., Lyon, G.L., Muehlenbachs, K., and Bohlke, J.K. (1990) Geochemistry of reduced gas related to serpentinization of the Zambales ophiolite, Philippines. *Applied Geochemistry*, 5, 625–630.
- Ankudinov, A.L. and Rehr, J.J. (1997) Relativistic calculations of spin-dependent X-ray absorption spectra. *Physical Review*, B56, R1712–1716.
- Augé, T. and Legendre, O. (1994) Platinum-group elements oxides from the Pirogues ophiolitic mineralization, New Caledonia: origin and significance. *Economic Geology*, 89, 1454–1468.
- Augé, T. and Maurizot, P. (1995) Stratiform and alluvial platinum mineralization in the New Caledonia ophiolite complex. *Canadian Mineralogist*, 33, 1023–1045.
- Azaroual, M., Romand, B., Freyssinet, P., and Disnar, J.-R. (2001) Solubility of platinum in aqueous solutions at 25 °C and pHs 4 to 10 under oxidizing conditions. *Geochimica et Cosmochimica Acta*, 65, 4453–4466.
- Barnes, I., LaMarche Jr., V.C., and Himmelberg, G. (1967) Geochemical evidence of present-day serpentinization. *Science*, 156, 830–832.
- Basinski, Z.S., Hume-Rothery, W., and Sutton, A.L. (1955) The lattice expansion of iron. *Proceedings of the Royal Society of London. Mathematical and Physical Sciences, Series A*, 229, 459–467.
- Byrne, R.H. (2003) Comment on “Solubility of platinum in aqueous solutions at 25 °C and pHs 4 to 10 under oxidizing conditions” by Mohamed Azaroual, Bruno Romand, Philippe Freyssinet, and Jean-Robert Disnar. *Geochimica et Cosmochimica Acta*, 67, 2509.
- Cabral, A.R. and Lehmann, B. (2003) A two-stage process of native palladium formation at low temperatures: Evidence from a palladium gold nugget (Gongo Soco iron ore mine, Minas Gerais, Brazil). *Mineralogical Magazine*, 67, 453–463.
- Cabri, L.J. (2002) The platinum-group minerals. In L.J. Cabri, Ed., *The Geology, Geochemistry, Mineralogy and Mineral Beneficiation of Platinum-Group Elements*. Canadian Institute of Mining and Metallurgy Special Vol. 54, p. 13–129.
- Cabri, L.J. and Feather, C.E. (1975) Platinum-iron alloys: A nomenclature based on

- a study of natural and synthetic alloys. *Canadian Mineralogist*, 13, 117–126.
- Cabri, L.J., Harris, D.C., and Weiser, T.W. (1996) Mineralogy and distribution of platinum-group mineral (PGM) placer deposits of the world. *Exploration and Mining Geology*, 5, 73–167.
- Cornell, R.M. and Schwertmann, U. (2003) *The Iron Oxides: Structure, properties, reactions, occurrences, and uses*, 664 p. Wiley-VCH, Weinheim.
- Eggleton, R.A. and Fitzpatrick, R.W. (1988) New data and revised structure model for ferrihydrite. *Clays and Clay Minerals*, 36, 111–124.
- Evans, D.M. (2002) Potential for bulk mining of oxidized platinum-group element deposits. *Transactions of Institute of Mining and Metallurgy*, 111, B81–86.
- Hattori, K. and Cabri, L.J. (1992) Origin of platinum-group mineral nuggets inferred from an osmium-isotope study. *Canadian Mineralogist*, 30, 289–301.
- Hattori, K.H. and Hamilton, S. (2008) Geochemistry of peat over concealed kimberlites in the Attawaiskat area, James Bay Lowlands, northern Canada. *Applied Geochemistry*, 23, 3767–3782.
- Hey, P.V. (1999) The effects of weathering on the UG2 chromitite reef of the Bushveld Complex, with special reference to the platinum-group minerals. *South African Journal of Geology*, 102, 251–260.
- Jedwab, J. (2004) “Irite” (Hermann, 1836/1841) from the Urals. *Mineralogical Magazine*, 68, 369–394.
- Karapinar, N. (2003) Magnetic separation of ferrihydrite from wastewater by magnetic seeding and high-gradient magnetic separation. *International Journal of Mineral Processing*, 71, 45–54.
- Legendre, O. and Augé, T. (1993) Présence d’un oxyde d’iridium naturel dans les concentrés platinifères de la région d’Antanambao-Manampotsy, Madagascar. *Comptes Rendus Académie des Sciences, Paris, Série II*, 316, 921–927.
- McDonald, I., Ohnenstetter, D., Ohnenstetter, M., and Vaughan, D.J. (1999) Palladium oxides in ultramafic complex near Lavatrafo, Western Andriamena, Madagascar. *Mineralogical Magazine*, 63, 345–352.
- O’Day, P.A., Rehr, J.J., Zabinsky, S.I., and Brown Jr., G.E. (1994) Extended X-ray absorption fine structure (EXAFS) analysis of disorder and multiple-scattering in complex crystalline solids. *Journal of American Chemical Society*, 116, 2938–2949.
- Oberthür, T., Weiser, T.W., and Gast, L. (2003) Geochemistry and mineralogy of platinum-group elements at Hartley Platinum Mine, Zimbabwe. *Mineralium Deposita*, 38, 344–355.
- Palandri, J.L. and Reed, M.H. (2004) Geochemical models of metasomatism in ultramafic systems: Serpentinization, rodingitization, and sea floor carbonate chimney precipitation. *Geochimica et Cosmochimica Acta*, 68, 1115–1133.
- Ramdohr, P. (1980) *The Ore Minerals and Their Intergrowths*, 2nd edition, 1205 p. Pergamon Press, Oxford.
- Ravel, B. (2001) ATOMS: Crystallography for the X-ray absorption spectroscopy. *Journal of Synchrotron Radiation*, 8, 314–316.
- Sader, J.A., Leybourne, M.I., McClenaghan, M.B., and Hamilton, S.M. (2007) Low-temperature serpentinization processes and kimberlite ground water signatures in the Kirkland Lake and Lake Timiskiming kimberlite fields, Ontario, Canada: Implications for diamond exploration. *Geochemistry: Exploration, Environment and Analysis*, 7, 3–21.
- Sassani, D.C. and Shock, E.L. (1998) Solubility and transport of platinum-group elements in supercritical fluids: Summary and estimates of thermodynamic properties for ruthenium, rhodium, palladium, and platinum solids, aqueous ions, and complexes to 1000 °C and 5 kbar. *Geochimica et Cosmochimica Acta*, 62, 2643–2671.
- Shcheka, G.G., Lehmann, B., and Solianik, A.N. (2005) Pd-bearing oxides and hydrated oxides in mertieite-II crystals from alluvial sediments of the Darya River, Aldan Shield, Russia. *Mineralogical Magazine*, 69, 981–994.
- Sleep, N.H., Meibom, A., Fridriksson, Th., Coleman, R.G., and Bird, D.K. (2004) H₂-rich fluids from serpentinization: Geochemical and biotic implications. *Proceedings of the National Academy of Sciences*, 101, 12818–12823.
- Vincent, L., Pierre, G., Michel, S., Robert, N., and Masson-Delmotte, V. (2007) Tree-rings and the climate of New Caledonia (SW Pacific): Preliminary results from Araucariaceae. *Palaeogeography, Palaeoclimatology, Palaeoecology*, 253, 477–489.
- Weiser, T.W. (2002) Platinum-group minerals (PGM) in placer deposits. In L.J. Cabri, Ed., *The Geology, Geochemistry, Mineralogy, and Mineral Beneficiation of Platinum-Group Elements*. Canadian Institute of Mining, Metallurgy, and Petroleum, Special Volume 54, 721–756.
- Westland, A.D. (1981) Inorganic chemistry of the platinum-group elements. In L.J. Cabri, Ed., *Platinum-Group Elements: Mineralogy, geology, recovery*. Canadian Institute of Mining, Metallurgy, and Petroleum, Special Volume 23, 5–18.
- Wood, S.A. (1991) Experimental determination of the hydrolysis constants of Pt²⁺ and Pd²⁺ at 25 °C from the solubility of Pt and Pd in aqueous hydroxide solutions. *Geochimica et Cosmochimica Acta*, 55, 1759–1767.
- Wood, S.A., Mountain, B.W., and Pan, P. (1992) The aqueous geochemistry of platinum, palladium and gold: Recent experimental constraints and re-evaluation of theoretical predictions. *Canadian Mineralogist*, 30, 955–982.
- Zabinsky, S.I., Rehr, J.J., Ankudinov, A., Albers, R.C., and Eller, M.J. (1995) Multiple scattering calculations of X-ray absorption spectra. *Physical Review B*, 52, 2995–3009.

MANUSCRIPT RECEIVED SEPTEMBER 2, 2009

MANUSCRIPT ACCEPTED DECEMBER 2, 2009

MANUSCRIPT HANDLED BY LAURENCE GARVIE